Applied Catalysis B: Environmental 189 (2016) 199–209

Contents lists available at ScienceDirect

Applied Catalysis B: Environmental

journal homepage: www.elsevier.com/locate/apcatb

Copper based materials for water-gas shift equilibrium displacement

Miguel N. Moreira[a], Ana M. Ribeiro[a], Adelino F. Cunha[a,*], Alírio E. Rodrigues[a], Maxim Zabilskiy[b], Petar Djinović[b], Albin Pintar[b,*]

[a] Laboratory of Separation and Reaction Engineering, Department of Chemical Engineering, Faculty of Engineering, University of Porto, Rua Dr. Roberto Frias s/n, 4200-465 Porto, Portugal
[b] Laboratory for Environmental Sciences and Engineering, National Institute of Chemistry, Hajdrihova 19, SI-1001 Ljubljana, Slovenia

ARTICLE INFO

Article history:
Received 17 November 2015
Received in revised form 5 February 2016
Accepted 22 February 2016
Available online 26 February 2016

Keywords:
Syngas
Sorption enhanced water-gas shift reaction
CuO/CeO_2
Carbon dioxide capture
Hydrotalcite

ABSTRACT

Water-gas shift reaction and sorption enhanced water-gas shift were studied over Cu-CeO_2 and Cu-HTlc catalysts in the temperature range between 125 and 295 °C. The catalysts were characterized by N_2 sorption, XRD, H_2-TPR and SEM techniques. Among the tested catalysts, copper supported on polyhedral ceria nanoparticles showed the highest activity, achieving 87.6% CO conversion. High dispersion of copper was identified as a catalyst property required for high WGS activity. During SE-WGS tests using either a multilayer arrangement of Cu-CeO_2 catalyst and K-HTlc sorbent, or Cu promoted hydrotalcite hybrid catalyst, nearly 70 mol% H_2 was obtained in the product gas stream during the initial transient period. Elevated pressure and surplus of steam in the feed increased the sorption capacity of K-HTlc, resulting in delayed CO_2 breakthrough. On the other hand, dilution of feed stream with inert gas (He) resulted in a dramatic decrease of sorbent's capacity leading to an early CO_2 breakthrough.

1. Introduction

The water-gas shift (WGS) reaction is used to decrease the carbon monoxide content in synthesis gas while simultaneously increasing concentrations of hydrogen and carbon dioxide ($CO + H_2O \leftrightarrow H_2 + CO_2$; $\Delta_r H^\circ = -41.2$ kJ/mol) [1,2]. The adjustment of synthesis gas is required for further processing, e.g. methanol synthesis.

At higher temperatures, WGS reaction kinetics are fast, however at an expense of a less favorable chemical equilibrium. At lower temperatures, the equilibrium is more favorable, but the reaction kinetics decrease. Therefore, the WGS reaction is carried out in two stages, at high and low temperatures, resulting in lowering carbon monoxide content below 0.3 vol.%.

Both traditional high and low temperature shift catalysts, Fe_2O_3-Cr_2O_3 and Cu-ZnO, respectively, are extremely pyrophoric when activated. Also, low thermal stability of Cu-ZnO catalyst prevents its application at high temperatures, whereas Fe_2O_3-Cr_2O_3 is not active at low temperatures. According to these drawbacks, intensive research was directed at highly active and expensive noble metal-based WGS catalysts, especially for fuel cell applications [3–5]. However, due to economic reasons, transition metals are much more applicable. Therefore, the improvement of copper-based catalytic system is highly required.

Cerium (IV) oxide is known as a catalyst support for WGS reaction due to its promoter effect [4] and maintaining the dispersion of the active metal phase [5]. Furthermore, presence of a Ce^{4+}/Ce^{3+} redox pair can significantly increase the catalytic activity in WGSR through the redox mechanism [6]. For instance, this effect can be enhanced through appropriate synthesis methods or by doping with lanthanides. The outstanding catalytic performance of nanoshaped CeO_2 (ceria nanorods and ceria nanocubes) was attributed to the predominant exposure of {1 0 0} and {1 1 0} lattice planes. Oxygen is more labile on these planes compared to {1 1 1} surface plane of polyhedral CeO_2 nanoparticles [7–9]. Activity of CeO_2 based catalysts largely depends on the metal used as active phase [10].

Copper was used as active phase by Li et al. [7] in the temperature range between 175 and 300 °C with a feed gas composition of 2 mol% CO, 10.7 mol% H_2O and He balance at a GHSV of 80,000 h^{-1}. At low reaction temperatures, a 5 at.% Cu-Ce(La)O_x material was tested; it was found that a small increase in the metal content is sufficient to exert activity changes in the WGS reaction. Hydrogen in the feed did not affect the product yields, whereas a high steam-to-carbon ration (R) was useful to increase CO conversion [11]. This type of catalyst is active up to 600 °C [12].

While ceria supports and Cu-CeO_2 catalytic materials were widely used and known for the application in WGS reaction for

* Corresponding authors.
E-mail addresses: afcunha@fe.up.pt (A.F. Cunha), albin.pintar@ki.si (A. Pintar).

http://dx.doi.org/10.1016/j.apcatb.2016.02.046
0926-3373/

hydrogen production, hydrotalcite (HTlc) and especially Cu promoted hydrotalcite (Cu-HTlc), to our best knowledge, have not been reported for this purpose until now. HTlc materials exhibit high specific surface area and thermal stability in addition to their specific property, such as the ability to adsorb CO_2, which can be exploited for achieving conversions above equilibrium values. CO_2 adsorption occurs due to basicity and for charge compensation in HTlc materials [13,14]. It is well documented that K promoted hydrotalcite (K-HTlc) materials are excellent for CO_2 sorption [13,15,16]; these solids have also stable capacity for cyclic operation and mechanical strength in the presence of excess steam. Previous studies have demonstrated that they can be applied to enhance conversion in the steam methane and ethanol reforming reactions [17,18].

The sorption-enhanced water-gas shift reaction SE-WGSR concept is the combination of reaction and adsorption in a single reactor packed with a mixture of catalyst and adsorbent, and is considered to be a promising method for producing pure hydrogen in a single step.

The production of hydrogen can be significantly improved by the use of the concept of SERP that has been described by Sircar et al. in 1995 [19,20] and Carvill et al. in 1996 [21]. The clout of SERP is that it displaces the normal equilibrium restrictions by *in situ* capture of one product during the transient period of a reaction. As a result, high amounts of a desired/specific product can be obtained, coupled with purities close to ultra-pure levels (<10 ppm). In addition, the reaction can be operated at a much lower temperature (cheaper metallurgy & heat exchanger equipment and cheaper product purification as well) than it would be necessary by a conventional catalytic reactor due to thermodynamic limits. In detail, the concept of SERP applied in our work, comparison of WGSR and SE-WGSR, is based on Le Chatelier Principle where the forward reaction in equilibrium is increased by selectively removing some of the reaction products (in our case carbon dioxide) from the reaction zone. SERP uses here a selective adsorbent (K-HTlc), admixtured with the catalyst (K-HTlc plus CuCe43) or directly as an ideal mixture where the catalyst support is the adsorbent too (a bi-functional hybrid material consisting of active Cu and HTlc adsorbent), for selective removal of a reaction product. It is important to stress that the high yielded conversion of reactants (carbon monoxide & water) to products (hydrogen & carbon dioxide) for the equilibrium-controlled WGSR is only obtained during the transition period; this means that under industrial conditions the adsorbent (K-HTlc) must be periodically regenerated (adsorbed carbon dioxide compound). Carbon dioxide is desorbed by using the principles of cyclic pressure swing adsorption (cyclic-PSA) [22], otherwise only conventional steady-state WGSR will be obtained. Once more, it must be pointed out that this aforementioned concept only runs well, if e.g. the SE-WGSR is operated under a cyclic mode like in a reactive pressure swing adsorption unit (RPSA) where at least two vessels allow the continuous production mode [23]. The cyclic mode requires the repeating of adsorption, rinse, depressurization, purge and repressurization steps.

In the present work, a comprehensive study was performed to investigate the catalytic properties for hydrogen production over Cu-CeO_2 catalysts via WGSR and catalytic/adsorptive properties for SE-WGSR when a catalyst was combined with a K-HTlc sorbent in a multilayer pattern arrangement. As a reference for SE-WGSR, Cu-HTlc hybrid material has been used.

2. Experimental

2.1. Catalyst synthesis

The materials used in this work are abbreviated according to support material and copper loading. For example, CeCu58 corresponds to a copper loading of 5.8 wt.% supported on CeO_2, and HTCu49 corresponds to a copper loading of 4.9 wt.% supported on HTlc.

CeO_2 supports were prepared by precipitation method. Briefly, 84 mL of aqueous solution containing 4.9 g of $Ce(NO_3)_3{\cdot}6H_2O$ (99% purity, Sigma-Aldrich) was added to 140 mL of 6 M (CeCu58) or 1 M (CeCu61) aqueous solution of NaOH (99% purity, Merck) under vigorous stirring in order to produce CeO_2 crystallites shaped as rods and polyhedra, respectively. The suspensions were stirred for 30 min at room temperature and transferred into a Teflon®-lined stainless steel autoclave and aged at 100 °C for 24 h. Obtained suspensions were centrifuged at 5000 rpm and washed with distilled water until reaching pH 7. Then, solids were freeze dried for 24 h and calcined in air at 400 °C for 3 h (heating ramp 120 °C/h).

During preparation of CeCu58 and CeCu61 solids, 2.4 g of CeO_2 was dispersed in 70 mL of distilled water and 589 mg of $Cu(NO_3)_2{\cdot}3H_2O$ (99.5% purity, Sigma-Aldrich) was added, which corresponds to the nominal loading of 6 wt.% of Cu. Then, 35 mL of 0.5 M Na_2CO_3 (99.999% purity, Merck) was added under vigorous stirring. Suspension was additionally stirred for 2 h at room temperature, filtered, washed with distilled water and dried in a freeze-dryer (Christ, model Alpha 1–2 LDplus) for 24 h. Finally, solids were calcined in air at 400 °C for 3 h (heating ramp 120 °C/h).

CeCu130 and CeCu43 catalysts were prepared by co-precipitation at room temperature. Water solution of Na_2CO_3 was added dropwise to water solutions of $Cu(NO_3)_2{\cdot}3H_2O$ and $Ce(NO_3)_3{\cdot}6H_2O$. The amount of $Cu(NO_3)_2$ water solution added was calculated to yield a final 4.3 (CeCu43) and 13 (CeCu130) wt.% CuO in obtained mixed oxide catalyst samples. The solutions were well mixed with a Ultra Turrax T50 mixer at a speed of 4000 rpm. The pH value of the solution was kept below 5.5. The formed precipitate was thoroughly washed with hot distilled water in order to remove undesired sodium ions, and dried overnight in an oven at 110 °C. Afterwards they were calcined for 4 h at 450 (CeCu130) and 550 °C (CeCu43), respectively.

A commercial hydrotalcite-like compound (HTlc) PURAL MG30 (aluminium magnesium hydroxide, with 70 mol% Al_2O_3) from Condea (now Sasol) was used as support material for copper [24]. The required amounts of $Cu(NO_3)_2{\cdot}3H_2O$ were dissolved in 200 mL of water. Hereafter, the pellets of HTlc support were added to this solution, and treated under heated ultrasonic environment at 100 °C during 2 h. The obtained suspensions were dried at 110 °C for 48 h, crushed using a grinding mill into a fine powder, and calcined for 48 h at 275 °C under a nitrogen flow of 50 Ncm^3/min. Finally, this HTCu49 sample was activated in pure hydrogen (30 Ncm^3/min) at 275 °C for 24 h. The reason why HTlc has been chosen as support material is that HTlc is a suitable CO_2 sorbent [24–26], and can be applied for many reforming processes [27–29].

2.2. Characterization of catalysts

Fresh and spent catalysts were analyzed by N_2 sorption using a Micromeritics Tristar II 3020 apparatus. Prior to measurements, samples were degassed in N_2 flow for 1 h at 90 °C, followed by 4 h at 180 °C in the Micromeritics SmartPrep Degasser. The specific surface areas were determined by the multi-point BET method.

X-ray diffractograms were recorded on a PANalytical X'pert PRO diffractometer using Cu Kα radiation (λ = 0.15406 nm). The scanned 2θ range was between 5 and 85° in 0.034° increments and 100 s measuring time at each increment. The average CeO_2 crystallite size was calculated from line broadening of characteristic (1 1 1) CeO_2 peak by using the Scherrer equation.

H_2-TPR measurements were performed using a Micromeritics AutoChem II 2920 apparatus with a 50 Ncm^3/min stream of 5% H_2/Ar as reducing agent. The samples were heated from −20 to 400 °C with a 5 °C/min ramp during analysis. A LN_2–isopropyl alco-

hol cold trap was mounted on exhaust in order to condense water vapor and remove it from the effluent gas mixture, before entering the TCD detector. Prior to TPR tests, catalysts were pretreated *in situ* in synthetic air (20.5% O_2/N_2).

CuO dispersion was determined with pulse N_2O decomposition at 90 °C with 10% N_2O/He on calcined (synthetic air), reduced (5% H_2/Ar) and degassed (He) catalyst samples. Decomposition of N_2O and formation of N_2 was monitored with a TCD detector (a LN_2 cold trap was mounted on exhaust in order to condense unreacted N_2O).

Surface morphology of the supported catalysts (fresh and spent) was analyzed using Supra 35 VP field emission scanning electron microscope (Carl Zeiss).

2.3. Reaction studies

Details about the reactor setup can be found in previous studies [30,31]. Catalytic experiments were performed between 125 and 295 °C with a H_2O to CO molar ratio of 4:1. Temperature increments were performed with a heating rate of 5 °C/min in pure He. The temperature inside the reactor (middle of the reaction zone) was monitored with a thermocouple. For all the measurements made in this work, an average reproducibility error of around ±5% should be taken into account.

The materials used were loaded into the reactor and thermally treated for 48 h at 275 °C under a N_2 flow of 50 Ncm^3/min. This was followed by activation in pure H_2 with a flowrate of 30 Ncm^3/min at 275 °C for 24 h. During the WGSR catalytic tests, each temperature increment was evaluated for at least 6 h time on stream to ensure stable operating conditions. The effects of temperature, flowrate (contact time) and presence of sorbent during reaction and after regeneration were investigated. The inlet molar flowrate of the reactant CO was in most of the experimental runs equal to $\dot{n}_{CO,0}$ = 0.446 mmol/min (10 Ncm^3/min). Then, the total molar flow rate of the reactants for a steam-to-carbon ratio (R) of 4 was 2.231 mmol/min (5 × 0.446 mmol/min) and for R = 1 was 3.568 mmol/min (8 × 0.446 mmol/min − 4 × 0.446 mmol/min for CO and 4 × 0.446 mmol/min for water). These two reactant flowrates were kept constant, while different inert gas flowrates were used (from 0 to 200 Ncm^3/min). For example, when an inert gas-to-carbon ratio (I) equals 10, an inert gas flowrate of 100 Ncm^3/min (inert gas molar flowrate of 4.46 mmol/min) was mixed with 0.446 mmol/min of CO in the feed.

The water conversion was estimated by the measured amounts of carbon dioxide formed during reaction (indirect method), in agreement with the overall WGSR equation; 1 mol of carbon dioxide formed may consume 1 mol of water. However, during the conducted WGSR, the compounds exiting the reactor were passed through a large water trap, then through a condenser (stainless steel heat exchanger consisting on a bundle of tubes) and finally through an ice-cooled trap using a Dewar. The unreacted liquid water was periodically collected in the two traps and analyzed on the amounts obtained. In most of the cases the estimated amounts of water did not deviate more than ±5% from the water collected in the traps.

Accordingly to the experimental procedures used in this work, the space time abbreviated with τ, is based on weight hourly space velocity (WHSV = mass flow $\dot{m}$ [kg/s]/catalyst mass m_{cat} [kg], in unit seconds) and varied from 1493 to 70696, due to different inert gas flow rates utilized.

To ensure total regeneration of the sorbent, a temperature increase equal to 50 °C was applied for all hybrid materials used during SERP [32]. During the regeneration period, an inert gas flow of 50 Ncm^3/min together with a water vapor flow of 40 Ncm^3/min was maintained. The CO_2 release was accurately followed at these conditions, ensuring total desorption. Hereafter an adjustment of the desired reaction conditions was done.

Prior to SE-WGSR experiments, the tubular reactor was packed with alternating layers of catalyst (4 × 0.5 g), sorbent (3 × 16.7 g) and activated overnight (approximately 12 h) with a mixture of He (molar flowrate of 2.231 mmol/min) and water (molar flowrate of 1.785 mmol/min) at 295 °C. Before starting the experimental runs, the regeneration stream was switched to the reactive mixture of CO ($\dot{n}_{CO,0}$ = 0.446 mmol/min)and H_2O ($\dot{n}_{H_2O,0}$ = 1.785mmol/min), corresponding to a steam-to-carbon ratio of R = 4, balanced with He stream of $\dot{n}_{inert,0}$ = 2.231mmol/min ($\dot{V}_{inert,0}$ = 50Ncm^3/min), corresponding to an inert gas-to-carbon ratio of I = 5.

Conversions of the reactants (CO and H_2O) were calculated as follows:

$$X_{CO}[\%] = \frac{\dot{n}_{CO,0} - \dot{n}_{CO}}{\dot{n}_{CO,0}} \cdot 100\%$$

$$X_{H_2O}[\%] = \frac{\dot{n}_{H_2O,0} - \dot{n}_{H_2O}}{\dot{n}_{H_2O,0}} \cdot 100\%$$

where $\dot{n}_{CO,0}$ and $\dot{n}_{H_2O,0}$ represent the molar flowrates of CO and H_2O in the feed, respectively. $\dot{n}_{CO}$ and $\dot{n}_{H_2O}$ are the outlet molar flowrates of these reactants. The molar fractions y_i (or partial pressures) were calculated for all species present in the outlet gas stream:

$$y_i = \frac{\dot{n}_i}{\sum_i^n \dot{n}_i} = \frac{p_i}{p_{total}}; p_{total} = \sum_i^n p_i$$

where $\dot{n}_i$ represents the molar flowrate of one species and $\sum_i^n \dot{n}_i$ represents the total molar flowrate of species in the outlet stream. Equilibrium CO conversion and reactant/product composition are provided in the supplementary information (Figs. S1 and S2).

The yield of species *i* was calculated from:

$$Y_i(\%) = \frac{\dot{n}_i - \dot{n}_{i,0}}{\dot{n}_{CO,0}} \frac{\nu_{CO}}{\nu_i} \cdot 100\% = \frac{\dot{n}_i}{\dot{n}_{CO,0}} \cdot 100\%$$

with $\dot{n}_{i,0}$ = 0 due to the absence of H_2 and CO_2 at the inlet, and the stoichiometric coefficient ν_i is defined as: $\nu_{CO} = \nu_{H_2O} = \nu_{H_2} = \nu_{CO_2} = 1$. The selectivity of species *i* can be obtained by:

$$S_i = \frac{Y_i}{X_{CO}}$$

Considering a carbon monoxide inlet of 10 mmol/min where full conversion is obtained, then in agreement with the stoichiometry of reaction the maximum hydrogen yield obtained for WGSR is $Y_{i,max}$ = (5 mmol/min H_2/10 mmol/min CO)·100% = 50% associated with a maximum selectivity of $S_{i,max}$ = 50%/100% = 0.5.

Hydrogen selectivities close to one can only be obtained during SE-WGS where in ideal case pure hydrogen is released during the transient period in an enhanced way (captured carbon dioxide does not appear in the stoichiometry). That means for a full conversion of carbon monoxide and a yield of hydrogen equal to 100%, $Y_{i,max}$ = (10 mmol/min H_2/10 mmol/min CO)·100% = 100%, a selectivity equal to one, $S_{i,max}$ = 1, is obtained.

3. Results and discussion

3.1. Characterization of materials

Table 1 summarizes the relevant physical-chemical properties of copper based catalysts before and after the WGSR tests.

The CeCu58 and CeCu61 catalysts exhibited BET specific surface area of 74 and 110 m^2/g, respectively. Differences in BET

Table 1
Morphological and redox properties of catalysts.

Catalyst	S_{BET} (m^2/g)	d_{pore} (nm)	[a]CuO dispersion (%)	Cu content (wt.%)	CeO_2 crystallite size (nm)	Ce^{4+} toCe^{3+} (%)
CeCu58	74; 57[b]	12.8; 15.3[b]	35.0; 9.5[b]	5.8	11	24.2
CeCu61	110; 70[b]	7.9; 11.6[b]	39.2; 35[b]	6.1	7.8	26.4
CeCu43	50; 36[b]	5.8; 6.1[b]	34.8; 24.9[b]	4.3	8.3	28.3
CeCu130	71; 28[b]	3.3; 7.7[b]	8.4; 7.8[b]	13.0	12.2	25.9
HTCu49	187	9	16[c]	4.9	/	/

[a] Based on pulse N_2O chemisorption on previously reduced catalysts.
[b] After WGSR test.
[c] Average crystallite size, evaluated from XRD analysis.

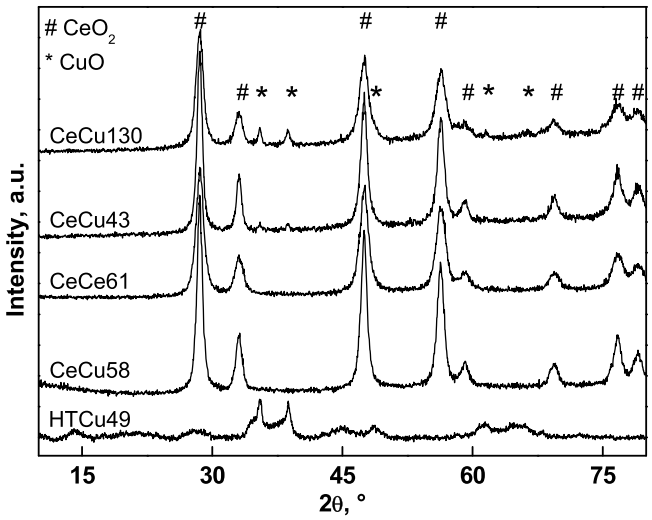

Fig. 1. XRD patterns of calcined copper containing CeO_2 and HTlc based catalysts prior to WGSR tests. Reflections belonging to CuO are highlighed with *, reflections belonging to CeO_2 are marked with #.

specific surface area originate from the morphology of the CeO_2 support. Namely, CeCu58 sample is comprised of ceria nanorods exposing (1 0 0) and (1 1 0) crystalline planes (S_{BET} = 87 m^2/g), whereas CeCu61 solid is based on polyhedral ceria exposing (1 1 1) crystalline planes (S_{BET} = 115 m^2/g). BET specific surface area of CeCu130 and CeCu43 samples was lower, namely 71 and 50 m^2/g, respectively. It was influenced also by the applied calcination temperature, which was 550 and 450 °C for CeCu43 and CeCu130 materials, respectively, compared to 400 °C, used for CeCu58 and CeCu61 samples. The BET specific surface area of HTCu49 material was 187 m^2/g.

The XRD patterns of prepared catalysts are presented in Fig. 1. Using the Scherrer equation, the crystallite size of CeO_2 in all synthesized CeCu catalysts was calculated to fall between 7.8 and 12.2 nm (Table 1). For CeO_2 based samples with a lower Cu content (CeCu43, CeCu58 and CeCu61), no other peaks besides those attributed to FCC fluorite type CeO_2 were detected (PDF 03-065-5923). This is due to the formation of very small clusters of CuO, which are finely dispersed over CeO_2 support [33]. For the CeCu130 catalyst containing 13 wt.% copper, peaks belonging to monoclinic CuO phase (PDF 00-005-0661) were also identified (Fig. 1), which can be attributed to the formation of crystalline CuO phase. XRD pattern of calcined HTCu49 catalyst exhibited diffuse diffraction maxima with much lower intensity, revealing lower extent of crystallinity. Only presence of CuO (PDF 00-005-0661) could be identified with certainty.

Morphology of the synthesized CeCu materials was investigated by scanning electron microscopy (SEM) and is depicted in Fig. S3. The CeCu58 catalyst consists of nanorods, which are up to 300 nm in length and 12–20 nm in diameter, whereas the CeCu61 catalyst consists of polyhedral crystallites. The identified morphology of CeO_2 is in accordance with higher alkalinity of the precipitating solution, which was used for the preparation of CeCu58 support. On the other hand, co-precipitated CeCu43 and CeCu130 samples are composed of lamellar platelets of CeO_2, with dimensions up to 1 μm (Figs. S3c and S3d). Segregated bulk CuO phase forms perforated structures, as can be seen in the upper right corner of Fig. S3d. This reveals that the formation of CuO takes place not only in the porous structure of CeO_2 support, but also outside of the pores, which consequently results in the formation of larger CuO particles and lower Cu dispersion.

Temperature programmed reduction was performed on copper based CeO_2 and HTlc catalysts prior to WGSR test (Fig. 2).

The close electronic and structural interaction between the CuO and CeO_2 phases (so-called "synergetic effect") causes formation of oxygen defects, enhanced oxygen mobility and reducibility [34]. Therefore, reduction of all analyzed binary oxides occurred at temperatures considerably lower than those of individual CuO and CeO_2 phases.

Reduction peaks in the temperature range below 100 °C (CeCu58, CeCu61 and CeCu43 samples) could be ascribed to reduction of finely dispersed copper and reduction of copper dimers or weak magnetic associates including clusters containing several copper ions [35,36]. Abovementioned Cu species are easily reducible, since strong interaction with ceria support significantly enhances CuO reducibility. This is in accordance with results of pulse N_2O chemisorption (Table 1), where high copper dispersion was found for these samples.

Between 100 and 150 °C co-reduction of CeO_2 phase and reduction of bulk CuO particles take place. The latter are weakly associated with CeO_2 and therefore reduction occurs at higher temperature compared with highly dispersed copper species [37]. This difference is especially noticeable for CeCu130 catalyst (reduction

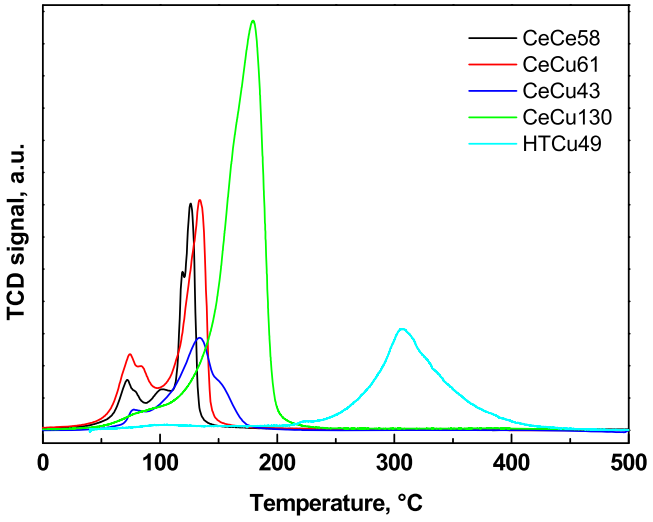

Fig. 2. H_2-TPR profiles of copper containing CeO_2 and HTlc based catalysts.

occurs mainly at temperatures above 150 °C). High Cu loading for this sample results in formation of bulk CuO phase (confirmed by N_2O chemisorption experiment as well as by XRD data, where peaks belonging to bulk CuO phase were found). Co-reduction of ceria support was observed for all the studied solids. Based on the quantification of H_2 consumed during TPR tests (for all the samples, quantity of utilized H_2 significantly exceeds the theoretical values, required for complete reduction of CuO phase to metallic Cu), amount of H_2 spent for CeO_2 co-reduction as well as extent of Ce^{+4} to Ce^{3+} reduction were calculated (Table 1). It should be noted that the extent of CeO_2 reduction does not depend on synthesis conditions and Cu loading, and is very similar for all examined catalysts (24.2–28.3%). Compared to CeCu catalysts, CuO reduction in HTCu49 sample occurs at higher temperatures, namely between 200 and 450 °C. This temperature range corresponds closely to pure CuO and reveals negligible redox interaction between copper clusters and HT support.

4.1. Catalytic performance

Conversions of CO and H_2O over CeCu and HTCu49 catalysts are shown in Fig. 3. Thermodynamic equilibrium conversions of CO and H_2O as a function of reaction temperature are included in Fig. S2.

As expected, CO and H_2O conversion increase with temperature. The product distribution is in agreement with the expected stoichiometry of the WGSR reaction, indicating that no side reactions occurred where carbon, methane or methanol are formed [38,39].

Among the examined CeO_2 based catalysts, CeCu61 and CeCu43 samples exhibited the highest activity. Both were based on polyhedral CeO_2 nanocrystallites. On the other hand, activity of CeCu58 and CeCu130 samples is lower. By comparing physical-chemical properties of fresh CeCu58 material and the one after WGSR test, significant decrease of CuO dispersion (from 35 to 9.5%) and copper sintering were observed after catalytic runs (Table 1). H_2-TPR profile of this sample after WGSR (Fig. S4) also confirms agglomeration of CuO nanoparticles in the bulk phase. Reduction occurred at significantly higher temperature compared to fresh material (mainly after 150 °C), which is typical for segregated CuO. At the same time, copper supported on polyhedral ceria nanoparticles (CeCu61, CeCu43 and CeCu130 samples) was more stable and resistant to particle aggregation. These results are in good agreement with the work of Yao et al. [40]. They have found that metallic Cu species (active sites for WGSR) are more stable on polyhedral ceria compared to nanorods and nanocubes CeO_2, and therefore aggregation of Cu phase is more pronounced for latter two morphologies. Therefore, observed activity of CeCu58 sample is significantly lower in comparison to polyhedral based samples (CeCu61 and CeCu43).

At the same time CeCu130 catalyst (containing 13 wt.% of Cu supported on polyhedral ceria) was characterized by poorly dispersed copper phase (confirmed by results of SEM, XRD, H_2-TPR and N_2O chemisorption experiments). This is crucial for water-gas shift reaction, where finely dispersed Cu species show the highest activity, whereas aggregated bulk copper phase is spectator species in this reaction [41]. Thus, CeCu130 catalyst showed inferior activity during WGSR tests.

In order to compare the activity of HTCu49 catalyst to CeO_2 based ones, tests under identical conditions were performed (Fig. 3e). CO conversions achieved with this hybrid catalyst increased from 20 to 40% when reaction temperature was raised from 125 to 175 °C. Upon further increase of reaction temperature, 67% CO conversion is ultimately reached at 295 °C. This is lower compared to CeCu61 and CeCu43 catalysts, which managed to reach values of 90 and 86% CO conversion, respectively. The excess of steam used (R = 4) does not affect substantially the conversion of water as it can be seen by the relatively low changes. However, it must be emphasized that for a 10% conversion of CO, only a conversion of 2.5% of water is obtained (according to the equation X_{CO} [%] = 4 × X_{H2O} [%]). By increasing flow of inert, contrarily to changes of CO conversion, the changes of water conversion are small. With increasing flowrate of inert gas, retention time was shortened, which resulted in an expected decrease of achieved CO conversions. This suggests the possibility of absence of external diffusion limitations in the lower flowrate regime. However, two variables change at a time, the flow rate and the residence time which can also influence the conversion.

Finally, another explanation with less probability of occurrence may also be considered for the differences in conversions obtained in the steady-state regime for different inert gas flow rates. According to Lavoisier, neither the total pressure nor the partial pressure of inert gas influences the single WGS reaction equilibrium. However, if a reaction scheme is considered with possible side reactions, such as the formation of methanol, then the results obtained from thermodynamic equilibrium calculations are different. Since the formation of methanol is a volume decrease reaction, conversion of carbon monoxide may decrease slightly with higher inert gas flow rates.

It seems that the WGS activity of the tested catalysts depends mainly on the copper cluster size and its stability during examined reaction conditions (Table 1). Catalysts with a low Cu content (CeCu43, CeCu58 and CeCu61) show high CuO dispersion as a result of very small CuO clusters dispersed over CeO_2 support. However, only CeCu43 and CeCu61 solids exhibit superior WGSR activity, while CeCu58 material is less active due to sintering of CuO clusters and formation of bulk CuO aggregates during catalytic runs. On the other hand, the CeCu130 catalyst shows the presence of crystalline CuO, which was confirmed by XRD, SEM and N_2O chemisorption analyses. As a result, activity of this sample is significantly lower compared to CeCu43 and CeCu61 catalysts.

The HTCu49 catalyst shows a copper crystallite size of 16 nm, as calculated by the Scherrer equation. However, very small metal clusters are invisible in XRD analysis. These are likely present and contribute importantly to the catalytic activity, especially since no synergetic redox assistance of CeO_2 is available. Considering the very high surface area of this material and low calcination temperature used, it is very likely that very small Cu clusters are present.

In the following paragraphs the use of SE-WGSR is discussed with the aim to follow the CO_2 breakthrough periods and to detect reaction enhancement in terms of CO conversion in the transient period by sorption of CO_2. The obtained results over the most active CeCu43 catalyst, combined with K-HTlc sorbent are plotted in mol percent of H_2 and CO_2 versus reaction time (Fig. 4).

Four regions are observed and depicted in Fig. 4a: (a) a transient start-up period, (b) a pre-breakthrough period, where WGSR runs at maximum efficiency, (c) a breakthrough period, where the efficiency of the adsorption reaction starts to decrease, and finally (d) a post-breakthrough period, where only the WGS reaction takes place. These regions can be extrapolated in the same analogy to Fig. 4b–d. A typical reactor response curve can be found in [42,43], whereas Harrison et al. [44] clearly describe the four regions of SERP. In this work, a pre-breakthrough interval of 10 min was determined. Finally, the onset of pre-breakthrough is 0% of CO_2 in the effluent.

The monitoring of the temperature (red curve associated to the right temperature axis in Fig. 4) was introduced to detect temperature variations during CO_2 capture by the sorbent. It is known that physical adsorption is a spontaneous and slightly exothermic process [45], and this can be observed (little temperature variation) from the red curves. The temperature that surges at later times, after adsorption, is almost steady indicating that no CO_2 adsorption is present anymore. Fluctuations or delays of the temperature, however, must be attributed to the PID regulation/temperature control.

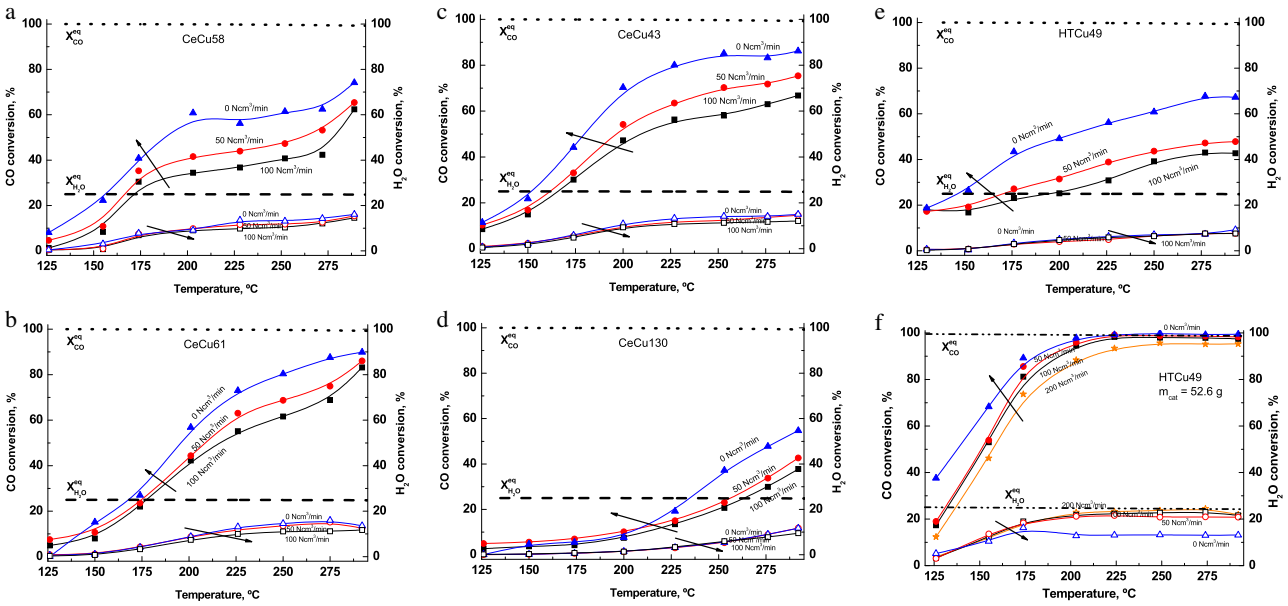

Fig. 3. CO and H_2O conversions as a function of reaction temperature at steady-state conditions over: (a) CeCu58, (b) CeCu61, (c) CeCu43, (d) CeCu130 catalysts, (e) and (f) HTCu49 sample. Operating conditions: m_{cat} = 2.0 g (a-e) and 52.6 g (f); p = 100 kPa.
$\dot{n}_{CO,0} = 0.446$ mmol/min; $\dot{n}_{H_2O,0} = 1.785$ mmol/min; R = 4; $\dot{V}_{inert,0} = 200 Ncm^3/\text{min}$, I = 20 (stars);
$\dot{n}_{CO,0} = 0.446$ mmol/min; $\dot{n}_{H_2O,0} = 1.785$ mmol/min; R = 4; $\dot{V}_{inert,0} = 100 Ncm^3/\text{min}$, I = 10 (squares);
$\dot{n}_{CO,0} = 0.446$ mmol/min; $\dot{n}_{H_2O,0} = 1.785$mmol/min; R = 4; $\dot{V}_{inert,0} = 50 Ncm^3/\text{min}$, I = 5 (circles);
$\dot{n}_{CO,0} = 0.446$ mmol/min; $\dot{n}_{H_2O,0} = 1.785$ mmol/min; R = 4; $\dot{V}_{inert,0} = 0 Ncm^3/\text{min}$, I = 0 (triangles).

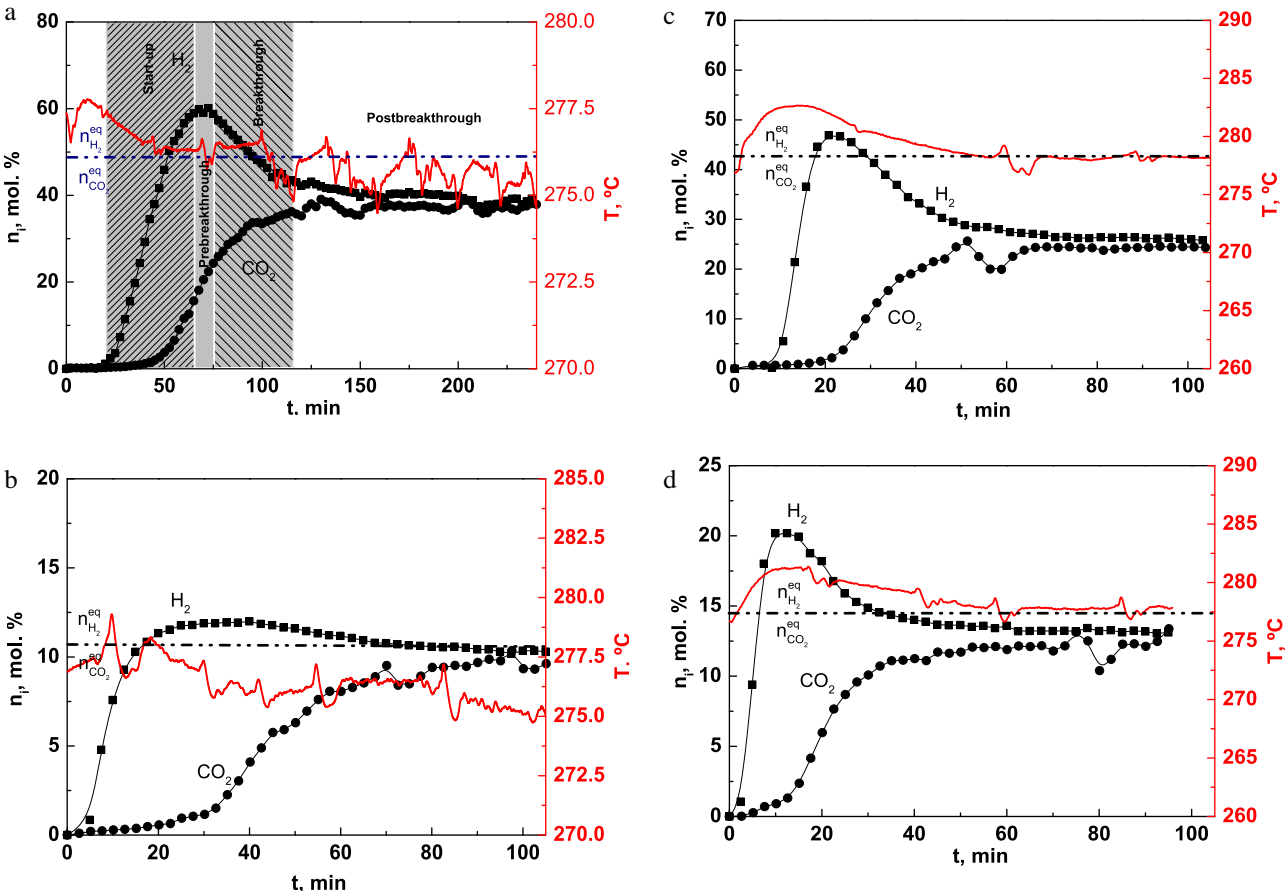

Fig. 4. Product distribution as a function of reaction time in a multilayer system consisting of CeCu43 catalyst ($m_{cat} = 4 \times 0.5$ g) and K-HTlc sorbent ($m_{sorb} = 3 \times 16.7$ g). Operating conditions: p = 100 kPa, T = 275 °C, $\dot{n}_{CO,0} = 0.446$ mmol/min.
(a) R = 4, $\dot{V}_{total,0} = 100 Ncm^3/\text{min}$, I = 0; (b) R = 4, $\dot{V}_{total,0} = 150 Ncm^3/\text{min}$, I = 5; (c) R = 1, $\dot{V}_{total,0} = 100 Ncm^3/\text{min}$, I = 0; (d) R = 1, $\dot{V}_{total,0} = 150 Ncm^3/\text{min}$, I = 5.

Table 2
Comparative performance between WGSR and SE-WGSR activity of CeCu catalysts.

Catalysts	Operating conditions					Transient state			Steady state			
	m_{cat} (g)	m_{sorb} (g)	T (°C)	p (kPa)	$\dot{V}_{inert}$ (Ncm^3/min)	X_{CO} (%)	Y_{H_2} (%)	S_{H_2} (/)	X_{CO} (%)	X_{H_2O} (%)	Y_{H_2} (%)	S_{H_2} (/)
CeCu58	2	/	275	100	0	–	–	–	62.5	14.3	n.a.	n.a.
CeCu61			275	100	0	–	–	–	87.6	11.1	45.2	0.5
CeCu130			275	100	0	–	–	–	47.8	6.0	26.3	0.5
CeCu43			275	100	0	–	–	–	82.7	11.0	38.7	0.5
CeCu43	4 × 0.5	3 × 16.7	275	100	0	85.4	59.3	0.7	82.7	11.0	38.7	0.5
and			275	100	50	82.3	59.5	0.7	81.8	12.2	41.0	0.5
K-			275	300	0	93.0	67.3	0.7	90.2	12.1	41.3	0.5
HTlc			275	500	0	97.7	69.5	0.7	92.6	12.5	42.9	0.5

m_{cat}/m_{sorb} = 0.04.

Table 3
Effect of feed H_2O/CO ratio on the SE-WGSR performance for alternating multilayer CeCu43 catalyst and K-HTlc sorbent formation.

Materials	Operating conditions				Transient state			Steady state			
	R	T (°C)	p (kPa)	$\dot{V}_{inert}$ (Ncm^3/min)	X_{CO} (%)	Y_{H_2} (%)	S_{H_2} (/)	X_{CO} (%)	X_{H_2O} (%)	Y_{H_2} (%)	S_{H_2} (/)
CeCu43	1	275	100	0	56.8	45.4	0.8	52.3	27.8	25.9	0.5
and	1	275	100	50	53.3	42.9	0.8	49.9	27.7	25.7	0.5
K-	4	275	100	0	85.4	59.3	0.7	82.7	11.0	38.7	0.5
HTlc	4	275	100	50	82.3	59.5	0.7	81.8	12.2	41.0	0.5

m_{cat}/m_{sorb} = 0.04.

The effect of SE-WGS becomes clear by comparing CO conversions at the transient and steady states (Fig. 4, Tables 2 and 3). H_2 content in the first 120 min of operation could be significantly increased compared to the steady-state operation, as shown in Fig. 4a. However, when the feed stream was diluted with inert gas (I = const. = 4; increase of R parameter from 0 to 5), the breakthrough time as well as the amount of H_2 generated were considerably reduced (Fig. 4a and b). The same situation was also observed with dilution of equimolar feed stream (Fig. 4c and d). The reason for lower efficiency of HTlc sorbent is because of the shorter contact times and lower steam-to-carbon ratio.

Since the experiments were conducted under excess steam, it is expected that the HTlc structure is maintained [46]. However, it was also found by Ficicilar and Dogu [47] that excess of water vapor could cause partial pore mouth closure, which increases the diffusion resistance for the transport of CO_2 to the active sites of the sorbent, leading to a lower CO_2 sorption capacity. Finally, He and water vapor can both act as regeneration gases for the hydrotalcite [13], resulting in lowering its capacity for CO_2 adsorption.

The effect of pressure in absence of any inert gas was also studied over the CeCu43 catalyst combined with K-HTlc sorbent arranged in alternating layers (Fig. 5). Since WGSR is an exothermic and volume neutral reaction, the variation of the total pressure does not directly affect the reaction equilibrium. However, it was expected that the sorption capacity of the HTlc material for CO_2 is significantly higher at elevated pressures [48], which will indirectly result in higher achievable CO conversions at elevated pressures. Indeed, improvement of the performance (compared to SE-WGSR at 100 kPa) through displacing the reaction equilibrium to the product side by prolonging the CO_2 pre-breakthrough period (from ~10 to 20 min) was observed at 300 and 500 kPa.

In previous works, CO_2 breakthrough experiments were conducted under relevant conditions to determine breakthrough capacity and sharpness of the adsorption front [49,50]. It was reported that at 28 bar and 400 °C, the breakthrough occurs 16 min after starting the feed and that the breakthrough CO_2 capacity was around 1.4 mmol/g in the first PSA cycle. At a total pressure of 1 bar, sorption capacities of up to 1.13 mmol/g have been identified for K-HTlc powder at 0.5 bar CO_2 and 0.5 bar H_2O [13].

Boon et al. [51] performed the breakthrough experiments with CO_2, H_2O and mixtures thereof yielded also kinetics of adsorption on K-promoted HTlc over a wide range of partial pressures, up to 24 bar and at 400 °C. A maximum capacity of 1.5 mmol/g have been measured, both for CO_2 and for H_2O. By increasing the total pressure from 100 to 500 kPa, an increase in CO_2 sorption capacity of around 25% can be expected. In this way it is possible to estimate how much of the HTlc's total capacity for CO_2 sorption was filled during WGSR experimental runs, together with an estimate how much more CO_2 can be adsorbed when pressure is increased to 300 and ultimately 500 kPa. In our work, 1.16 and 1.19 mmol/g of CO_2 are estimated to be adsorbed at 300 and 500 kPa, respectively.

Finally, the deviation from the theoretical S-shape breakthrough curves observed at the tail (Fig. 5) can generally be attributed to heat effects [50]. Normally an exotherm or thermal front with a specific wave velocity travels along the bed that is associated to the adsorption reaction front. The temperature falls gradually toward its initial value when the adsorption front has passed.

Isothermal SE-WGSR performance of the hybrid HTCu49 catalyst is shown in Fig. 6. Tests were performed at conditions identical to those used in Fig. 4a. Mass of the hybrid catalyst, however, was adjusted to contain 2 g of copper (active WGSR catalyst component), which resulted in 52.6 g of hybrid catalyst.

It can be seen in Fig. 6a that for the hybrid HTCu49 catalyst it is quite difficult to surpass the thermodynamic equilibrium during transient mode, meaning that a SERP is almost impossible, while for the combination of HTCu49 hybrid catalyst (3 × 17.53 g) plus K-HTlc sorbent (2 × 16.6 g) also in a multilayer pattern arrangement, check Fig. 6b–d, the performance is much better.

Concentration profile of CO_2, in Fig. 6b, was trailing behind the one of H_2 and reveals its fixation on the hybrid catalyst. The H_2 content/yield in the first 35–45 min of reaction when CO_2 sorption occurs is only slightly higher (65.3% compared to 48.2%) than in the steady-state operation (75–240 min). However, in the experimental tests depicted in Fig. 4a (multilayer arrangement of CeCu43 catalyst and K-HTlc sorbent) and Fig. 6b (multilayer arrangement of HTCu49 hybrid catalyst and K-HTlc sorbent) CO_2 appears only after 50 min, while in Fig. 6a (HTCu49 hybrid catalyst) this occurs after 25 min. The reason why the capacity is so much lower, is that in the former cases a K-promoted HTlc has been used as

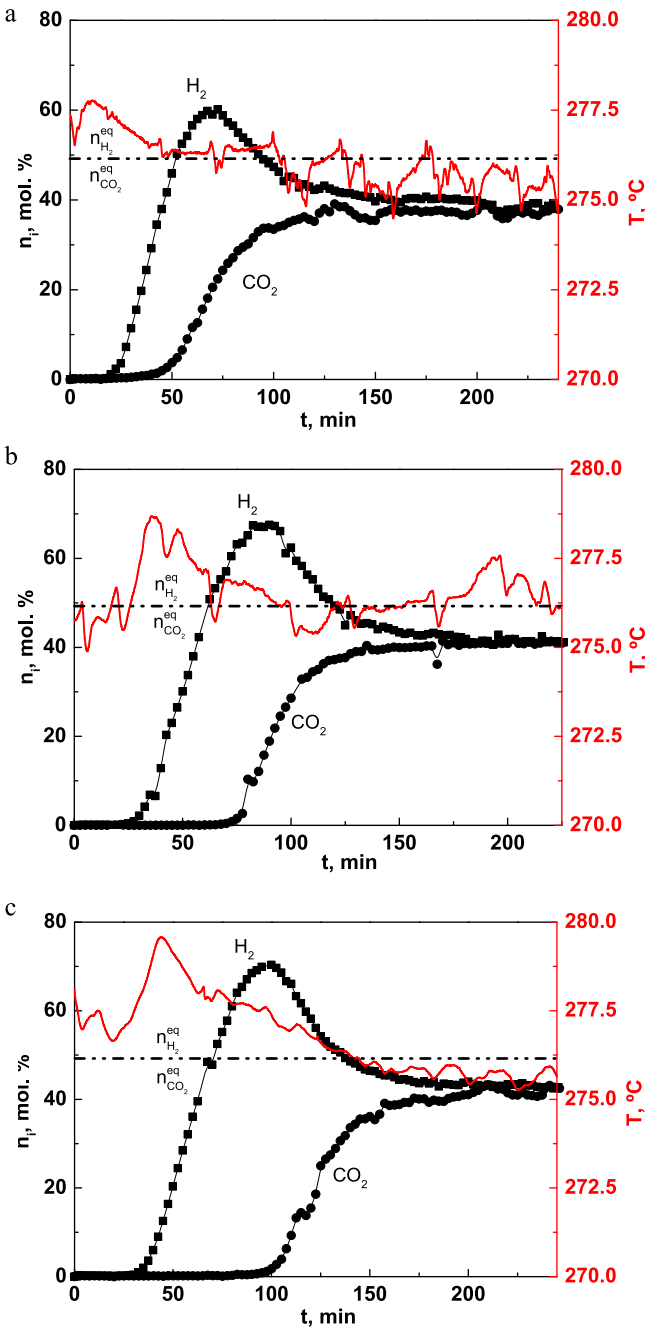

Fig. 5. Product distribution as a function of reaction time in a multilayer system consisting of CeCu43 catalyst ($m_{cat} = 4 \times 0.5$ g) and K-HTlc sorbent ($m_{sorb} = 3 \times 16.7$ g) at T = 275 °C, $\dot{n}_{CO,0} = 0.446$ mmol/min, R = 4, I = 0, $\dot{V}_{total,0} = 100 Ncm^3/$ min: (a) p = 100 kPa; (b) p = 300 kPa; (c) p = 500 kPa.

selective CO_2 sorbent with a sorption capacity of q = 0.75 mmol/g (T = 400 °C, p_{total} = 200 kPa, p_{CO2} = 40 kPa in the presence of water vapor) [26,30], while in the latter case an unpromoted or pure HTlc was used with a sorption capacity of q = 0.1 mmol/g [31]. The presence of copper does not affect the CO_2 sorption capacity of promoted, nor non-promoted HTlc [24]. As a result, the inferior adsorption property manifests also through a much lower H_2 concentration.

That can be also seen indirectly for the conversion of CO (Fig. 6c) and yields obtained (Fig. 6d). It is obvious that the SERP region is identified between 0 and around 125 min (Fig. 6d), which is in relatively good agreement with the plots in Fig. 6b and c demonstrating an overlapping between the SERP region and yields of H_2 and CO_2 as well as conversions of CO and water.

The operating condition resulted in the following steady-state values: 99.4% CO and 11.6% water conversion, 48.2% of H_2 yield and a selectivity of 0.49. On the other hand, the transient state had a better performance with the following values: 99.3% CO conversion and 65.3% H_2 yield with a selectivity of 0.66. The surplus here lies clearly in the gain of higher H_2 yields (transient state: $Y(H_2) = 65.3\%$; steady state: $Y(H_2) = 48.2\%$). These values can be consulted in Table 4 that are linked directly to Fig. 6. The enhancement in H_2 production is a result of the HTlc (K-HTlc), responsible for the CO_2 capture.

The most relevant results of transient and steady-state SE-WGSR reaction are summarized in Tables 2–4. The values have been obtained for the best performances (highest yield of H_2) for an average time interval of 10 min. The use of CeCu43 catalyst and K-HTlc sorbent in a multilayer arranged pattern shows better performances (in terms of higher CO conversion and H_2 yield) in the transient period compared to the steady-state periods, which is the main benefit over the pure catalytic system (Table 2).

However, the introduction of inert in the feed ($I \neq 0$) decreases also the performance of the hybrid catalytic system in the transient state due to the lower contact time (Table 2).

At elevated pressure, the advantage of using a hybrid catalyst for SE-WGSR becomes even more prominent, as CO_2 breakthrough can be prolonged by a factor of 2 (Fig. 5a and c). Catalytic activity is also better when an inlet feed of R = 4 is used. This is because a considerable surplus of water in the feed results in small kinetic limitations at high CO conversions. In addition to the continuous removal of produced CO_2 from the gas stream by the HTlc sorbent, considerable increase of CO conversions compared to equimolar feed compositions (or regular WGSR) can be achieved.

At this point, it is convenient to discuss the performance of the hybrid material HTCu49 during transient state and steady state (Table 4), as well as the comparison between HTCu49 hybrid catalyst and CeCu43 multilayer arrangement.

The use of the HTCu49 hybrid material plus K-HTlc sorbent shows performance improvements (in terms of higher CO conversion and H_2 yield), if the transient period is compared with the steady-state period. However, the obtained improvements are lower in comparison to the previously discussed multilayer pattern system of CeCu43 and K-promoted HTlc. As an example, at a temperature of 275 °C and a pressure of 500 kPa, the results obtained in the transient period were $X_{CO} = 99.8$, $Y(H_2) = 68.6$ and $S(H_2) = 0.69$, which are higher compared to the steady-state period with values of $X_{CO} = 99.8$, $Y(H_2) = 49.4$ and $S(H_2) = 0.50$. This means that the differences obtained between the transient state and steady state are as follows: $\Delta X_{CO} = 0\%$, $\Delta Y(H_2) = 9.2\%$ and $\Delta S(H_2) = 0.19$. These differences compared to those obtained for the multilayer pattern system consisting of CeCu43 and K-promoted HTlc are indeed greater, as it was calculated with the following results obtained: $\Delta X_{CO} = 5.1\%$, $\Delta Y(H_2) = 29.4\%$ and $\Delta S(H_2) = 0.27$. The results of the multilayered arrangement of CeCu43 catalyst and K-promoted HTlc sorbent are superior to that of HTCu49 hybrid catalyst due to the effect of higher sorption capacity of the K-promoted HTlc, and to that of HTCu49 hybrid catalyst and K-promoted HTlc sorbent due to the lower total mass of sorbent used (2×16.6 g).

A stable bed of catalyst plus sorbent was observed after CO_2 release by temperature swing, and that is of course the key step for validation of the results obtained that contribute to a possible industrial application [32].

It is correct that the performance of the Cu-HTlc hybrid material is poor in comparison to the combined Cu-CeO_2 catalyst and K-HTlc sorbent, or Cu-HTlc hybrid material and K-HTlc sorbent. However, it can be used as a reference for SE-WGSR. The reason of using a more

Table 4
SE-WGSR performance for the hybrid HTCu49 catalyst plus K-HTlc sorbent at different pressures.

Material	Operating conditions					Transient state			Steady state			
	m_{cat} (g)	$m_{sorbent}$ (g)	T (°C)	p (kPa)	$\dot{V}_{inert}$ (Ncm^3/min)	X_{CO} (%)	Y_{H_2} (%)	S_{H_2} (/)	X_{CO} (%)	X_{H_2O} (%)	Y_{H_2} (%)	S_{H_2} (/)
HTCu49	3 × 17.5	2 × 16.6	275	100	0	99.3	67.2	0.7	99.4	13.3	45.3	0.5
and			275	100	50	99.3	100.0	0.7	96.6	12.9	55.5	0.5
K-			275	300	0	99.8	68.6	0.7	99.8	10.6	45.8	0.5
HTlc			275	500	0	99.8	68.6	0.7	99.8	11.4	49.4	0.5

$m_{Cu}/m_{HTlc} = 0.052$.

Table 5
Selected results reported in the literature for WGSR reaction.

Catalyst	τ (s)	T (°C)	p (kPa)	$\dot{n}_{CO,0}$ (mol.%)	R (mol/mol)	X_{CO} (%)	X_{H_2O} (%)	Y_{H_2} (%)	S_{H_2} (/)	[c]$X_{CO,eq}$ (%)	Reference
6.1% Cu/ZrO_2	1283.1[b]	270	100	15	2.6	88.1	–	–	–	–	[55]
Pd-Cu/CeO_2	0.056[a]	260	100	9.7	2.4	69.4	–	–	–	–	[61]
$Cu/ZnO{\cdot}Al_2O_3$	3251.1[b]	250	100	15	1	95.4	–	–	–	–	[62]
Cu/CeO_2	0.71[a]	303	100	5	3	68.9	–	–	–	–	[67]
Cu/ZrO_2	0.9[a]	250	100	10	1	92.4	–	–	–	–	[71]
CeCu58	2688[b]	275	100	20	4	62.5	14.3	58.1	0.93	99.4	[This Work]
CeCu61	2688[b]	275	100	20	4	87.6	11.1	45.2	0.52	99.4	[This Work]
CeCu43	2688[b]	275	100	20	4	82.7	9.9	42.6	0.52	99.4	[This Work]
CeCu130	2688[b]	275	100	20	4	47.8	6.0	26.3	0.55	99.4	[This Work]
HTCu49	2688[b]	275	100	20	4	67.3	7.6	31.9	0.47	99.4	[This Work]
HTCu49	64268[b]	275	100	20	4	95.2	13.0	53.3	0.56	99.4	[This Work]
HTCu49	64268[b]	275	100	10	4	98.6	20.9	90.9	0.54	99.4	[This Work]

[a] $\tau_{GHSV} = (GHSV)^{-1}$.
[b] $\tau_{WHSV} = (WHSV)^{-1}$.
[c] WGSR equilibrium.

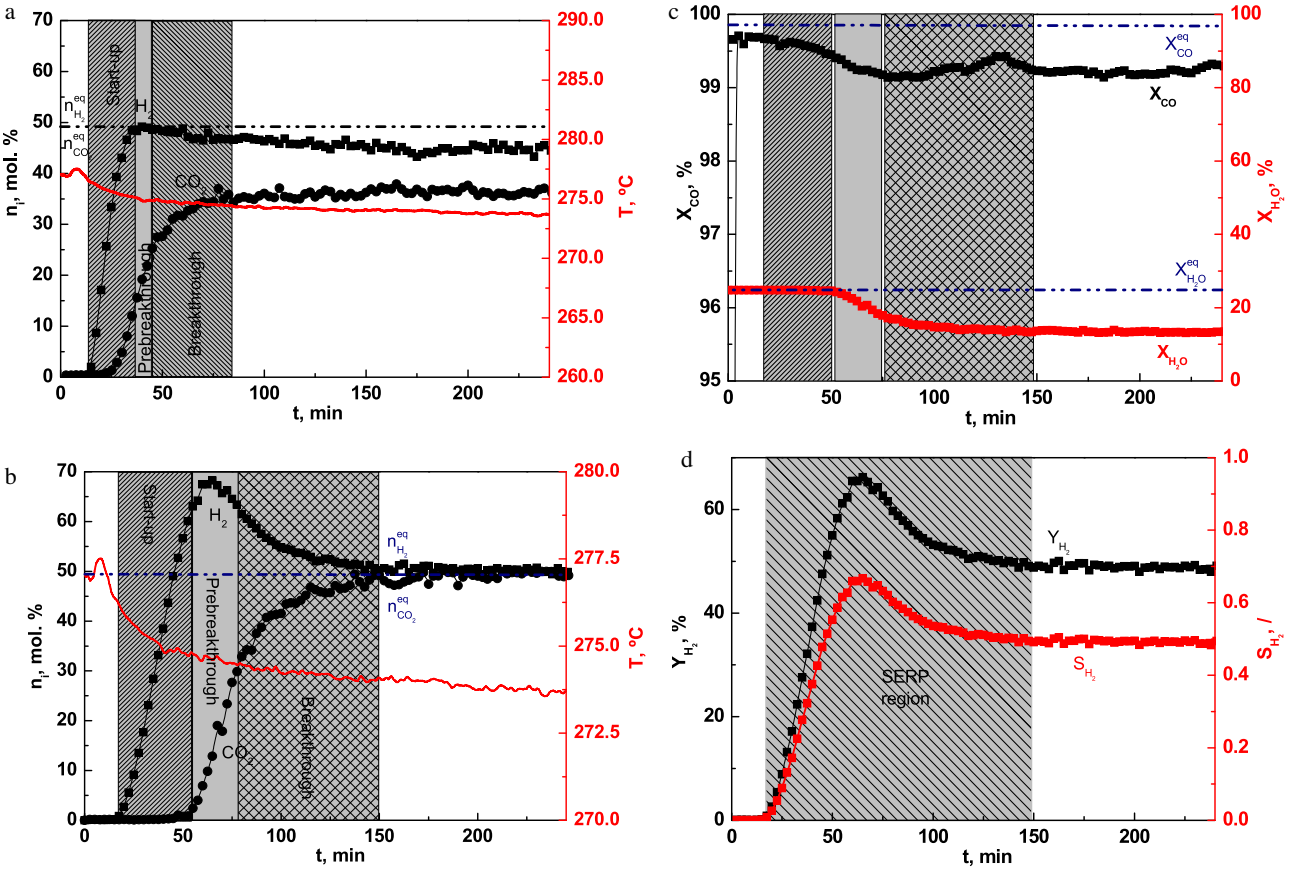

Fig. 6. Product distribution (a) as a function of reaction time for the hybrid catalyst HTCu49 ($m_{cat} = 1 \times 52.6$ g). Product distribution (b), CO conversion (c) and H_2 yield & selectivity (d) as a function of reaction time for the hybrid catalyst HTCu49 ($m_{cat} = 3 \times 17.53$ g) and K-HTlc sorbent ($m_{sorb} = 2 \times 16.6$ g). Operating conditions: T = 275 °C, $\dot{n}_{CO,0} = 0.446$mmol/min, R = 4, I = 0 and p = 100 kPa.

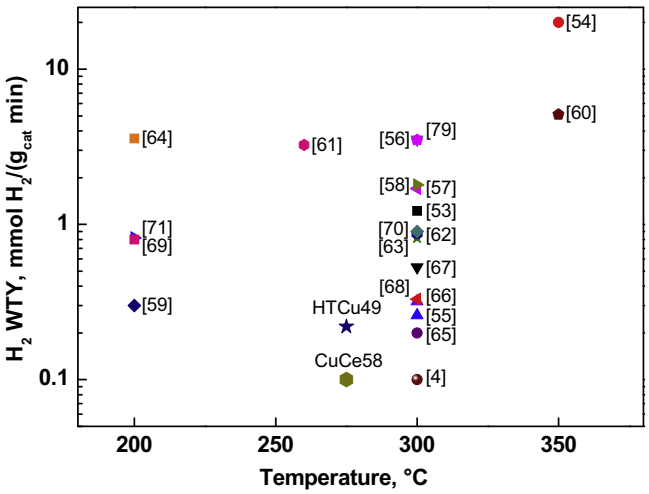

Fig. 7. Hydrogen weight-time yield (H_2 WTY) as a function of reaction temperature based on results reported in literature and this work.

complex system (catalyst and sorbent) is to ensure that for a future work a novel hybrid material consisting of Cu as active phase, CeO_2 as redox-promoter and K-HTlc as catalyst support and selective carbon dioxide adsorbent may perform at least similar but expecting higher performances on SE-WGSR such as high yielding of ultrapure hydrogen at lower temperatures. Finally, it is also objective to ensure the proof-of-principle for the concept of SERP applied on SE-WGSR. The essence here is that both the selective adsorbent (K-HTlc), admixture with the catalyst (K-HTlc plus CuCe43) or ideal mixture where the catalyst support is the adsorbent too (a bi-functional hybrid material consisting of active Cu and HTlc adsorbent), for selective removal of a reaction product can operate similarly so that for an industrial application the future customers have more than one alternative to pack the RPSA unit.

What follows is the comparison of results obtained in the present study with those previously reported for the WGSR reaction over copper-based catalysts at steady-state conditions [52–71] (Table 5 and S2). At this point it must be stressed that experimental conditions (especially reaction temperature) collected from literature (Table S2), differ too much to make a simple CO conversion comparison, yet they are helpful for a future adjustment in the choice of selective CO_2 adsorbents [72].

Results of this work can be compared with other research groups by introducing the criterium of hydrogen weight-time yield, abbreviated as H_2 WTY in the y-axis of the graph of Fig. 7.

It can be seen that the support material used influences strongly the performance; zinc oxide and mixtures of zinc oxide with alumina show excellent perfomances, perhaps similar to those of cerium oxide based catalysts at temperatures around 300 °C. The reason why this support material is so well established is that an interacting synergy between Cu and ZnO should be taken into account [1,73]. Cerium oxide based support materials also perform very well, especially in the lower temperature ranges due to their capacity for oxygen mobility [2,7].

As a final conclusion one can predict that SERP applied to SE-WGSR using a cyclic RPSA unit may work perfectly since the Energy Research Centre of the Netherlands [49,74] has scaled-up the process into a pilot plant with success. It is also known that industrial copper-based catalysts work quite stable if an operation temperature lower than 300 °C is used [1,75]. Then, for both the cyclic regeneration and the reaction temperature, the overall operating temperature below 300 °C must be ensured to almost completely avoid sintering of copper particles (Tamman Huetig criterium) [24,73,76–80].

4. Conclusions

Sorption enhanced WGS reaction was investigated over hybrid HTCu49 (copper on hydrotalcite) and various CeCu (copper on CeO_2) catalysts. At low temperatures (between 125 and 175 °C), HTCu49 hybrid catalyst was most active achieving between 20 and 40% CO conversion, likely due to its CO_2 sorption capacity which minimized kinetic limitations associated with high CO conversions. However, comparing HTCu49 and CeCu43 samples that have similar loadings when a catalyst mass of 2.0 g was used for both, conversions of CO are close to each other, emphazising clearly that the amount of active copper dictates the catalyst activity for WGSR. At temperatures above 175 °C, CeCu61 and CeCu43 catalysts exhibited the highest activity, reaching CO conversions of 87.6 and 82.7% at 275 °C, respectively. High dispersion of copper was identified as a required catalyst property to obtain high WGS activity. In a multilayer arrangement of CeCu43 catalyst and K-HTlc sorbent, CO_2 was efficiently removed from the effluent stream resulting in significant increase of CO conversion and H_2 enrichment of up to 70 vol.% in the transient operation, compared to steady-state operation. The benefit of SE-WGS towards WGS was successfully demonstrated in the transient mode of operation. Upon increasing the pressure of SE-WGS reaction from 100 to 500 kPa, the sorption capacity of K-HTlc was improved by around 25%, resulting in prolongation of CO_2 pre-breakthrough time from 10 to 20 min. In addition to pressure, steam surplus was discovered to positively affect the CO_2 sorption capacity of the K-HTlc sorbent, delaying CO_2 breakthrough and prolonging the transient operation time window. On the other hand, dilution of feed stream with inert (He) resulted in a dramatic decrease of sorbent's capacity for CO_2, which resulted in an early CO_2 breakthrough.

Acknowledgements

The authors acknowledge financial support provided by Fundação para a Ciência e a Tecnologia (FCT, Portugal) and FEDER under Programme COMPETE through the Project FCOMP-01-0124-FEDER-027458 (Ref[a]. FCT EXCL/QEQ-PRS/0308/2012). The authors also acknowledge the financial support of the Ministry of Education, Science and Sport of the Republic of Slovenia through research programme No. P2-0150. This work was co-financed by FCT/MEC and FEDER under Programme PT2020 (Project UID/EQU50020/2013). This work was also co-financed by QREN, ON2 and FEDER (Project NORTE-07-0162-FEDER-000050 and Project NORTE-07-0124-FEDER-0000007). We also acknowledge for the free available software provided by the Martin-Luther-Universität Halle-Wittenberg, Zentrum für Ingenieurwissenschaften (Prof. Dr. Dieter A. Lempe), and Hochschule Merseburg (FH), University of Applied Sciences, FB Ingenieur- und Naturwissenschaften (Prof. Dr. Gerd Hradetzky), entitled as "Thermodynamics of (Complicated) Chemical Reaction Equilibria", weblink: http://physchem.hs-merseburg.de/.

Appendix A. Supplementary data

Supplementary data associated with this article can be found, in the online version, at http://dx.doi.org/10.1016/j.apcatb.2016.02.046.

References

[1] C. Ratnasamy, J.P. Wagner, Water gas shift catalysis, Catal. Rev. 51 (2009) 325–440.
[2] P. Smirniotis, K. Gunugunuri, Water Gas Shift Reaction: Research Developments and Applications, Elsevier Science, 2015.
[3] R. Radhakrishnan, R.R. Willigan, Z. Dardas, T.H. Vanderspurt, AIChE J. 52 (2006) 1888–1894.

[4] H. Kušar, S. Hočevar, J. Levec, Appl. Catal. B 63 (2006) 194–200.
[5] H.S. Gandhi, M. Shelef, The role of research in the development of new generation automotive catalysts, in: A. Crucq, A. Frennet (Eds.), Studies in Surface Science and Catalysis, Elsevier, 1987, pp. 199–214.
[6] G. Jacobs, B.H. Davis, Low temperature water-gas shift catalysts Catalysis, vol. 20, The Royal Society of Chemistry, 2007, pp. 122–285.
[7] Y. Li, Q. Fu, M. Flytzani-Stephanopoulos, Appl. Catal. B 27 (2000) 179–191.
[8] S. Liang, G. Veser, Catal. Lett. 142 (2012) 936–945.
[9] M. Zabilskiy, P. Djinović, E. Tchernychova, O.P. Tkachenko, L.M. Kustov, A. Pintar, ACS Catal. 5 (2015) 5357–5365.
[10] E.T. Saw, U. Oemar, X.R. Tan, Y. Du, A. Borgna, K. Hidajat, S. Kawi, J. Catal. 314 (2014) 32–46.
[11] K. Liu, C. Song, V. Subramani, Hydrogen and Syngas Production and Purification Technologies, Wiley, 2016, pp. 2009.
[12] X. Qi, M. Flytzani-Stephanopoulos, Ind. Eng. Chem. Res. 43 (2004) 3055–3062.
[13] Y.J. Wu, P. Li, J.G. Yu, A.F. Cunha, A.E. Rodrigues, Chem. Eng. Technol. 36 (2013) 567–574.
[14] Y.J. Wu, F. Díaz Alvarado, J.C. Santos, F. Gracia, A.F. Cunha, A.E. Rodrigues, Chem. Eng. Technol. 35 (2012) 847–858.
[15] F. Cavani, F. Trifirò, A. Vaccari, Catal. Today 11 (1991) 173–301.
[16] N. Chanburanasiri, A.M. Ribeiro, A.E. Rodrigues, N. Laosiripojana, S. Assabumrungrat, Energy Fuels 27 (2013) 4457–4470.
[17] K.D. Dewoolkar, P.D. Vaidya, Energy Fuels 29 (2015) 3870–3878.
[18] Y.-J. Wu, P. Li, J.-G. Yu, A.F. Cunha, A.E. Rodrigues, Ind. Eng. Chem. Res. 53 (2014) 8515–8527.
[19] J.R. Hufton, S. Mayorga, S. Sircar, AIChE J. 45 (1999) 248–256.
[20] S. Sircar, M. Anand, B.T. Carvill, J.R. Hufton, S. Mayorga, R.N. Miller, Sorption enhanced reaction process for production of hydrogen, Hydrogen Program Rev. Proc. U.S. DOE (1995).
[21] B.T. Carvill, J.R. Hufton, M. Anand, S. Sircar, AIChE J. 42 (1996) 2765–2772.
[22] K.B. Lee, Sorption Enhanced Reaction Concepts For Hydrogen Production: Materials & Processes, Research Signpost, 2016, pp. 2010.
[23] Kulprathipanja, Reactive Separation Processes, CRC Press, 2001.
[24] A.F. Cunha, Y.J. Wu, J.C. Santos, A.E. Rodrigues, Chem. Eng. Res. Des. 91 (2013) 581–592.
[25] N. Chanburanasiri, A.M. Ribeiro, A.E. Rodrigues, N. Laosiripojana, S. Assabumrungrat, Energy Fuels 27 (2013) 4457–4470.
[26] E.L.G. Oliveira, C.A. Grande, A.E. Rodrigues, Sep. Purif. Technol. 62 (2008) 137–147.
[27] Y.-J. Wu, P. Li, J.-G. Yu, A.F. Cunha, A.E. Rodrigues, Chem. Eng. Sci. 118 (2014) 83–93.
[28] Y. Ding, E. Alpay, Chem. Eng. Sci. 55 (2000) 3929–3940.
[29] E.R. van Selow, P.D. Cobden, A.D. Wright, R.W. van den Brink, D. Jansen, Energy Procedia 4 (2011) 1090–1095.
[30] A.F. Cunha, Y.J. Wu, F.A. Díaz Alvarado, J.C. Santos, P.D. Vaidya, A.E. Rodrigues, Can. J. Chem. Eng. 90 (2012) 1514–1526.
[31] Y.-J. Wu, J.C. Santos, P. Li, J.-G. Yu, A.F. Cunha, A.E. Rodrigues, Can. J. Chem. Eng. 92 (2014) 116–130.
[32] A.F. Cunha, M.N. Moreira, A. Mafalda Ribeiro, A.P. Ferreira, J.M. Loureiro, A.E. Rodrigues, Energy Technol. 3 (2015) 1205–1216.
[33] P. Djinović, J. Batista, A. Pintar, Catal. Today 147 (2009) S191–S197.
[34] K. Zhou, R. Xu, X. Sun, H. Chen, Q. Tian, D. Shen, Y. Li, Catal. Lett. 101 (2005) 169–173.
[35] X. Yao, F. Gao, Q. Yu, L. Qi, C. Tang, L. Dong, Y. Chen, Catal. Sci. Technol. 3 (2013) 1355–1366.
[36] M. Zabilskiy, P. Djinović, B. Erjavec, G. Dražić, A. Pintar, Appl. Catal. B: Environ. 163 (2015) 113–122.
[37] X. Ma, X. Feng, X. He, H. Guo, L. Lv, J. Guo, H. Cao, T. Zhou, Microporous Mesoporous Mater. 158 (2012) 214–218.
[38] E. Xue, M. O'Keeffe, J.R.H. Ross, Catal. Today 30 (1996) 107–118.
[39] J. Xu, G.F. Froment, AIChE J. 35 (1989) 88–96.
[40] S.Y. Yao, W.Q. Xu, A.C. Johnston-Peck, F.Z. Zhao, Z.Y. Liu, S. Luo, S.D. Senanayake, A. Martinez-Arias, W.J. Liu, J.A. Rodriguez, Phys. Chem. Chem. Phys. 16 (2014) 17183–17195.
[41] R. Si, J. Raitano, N. Yi, L. Zhang, S.-W. Chan, M. Flytzani-Stephanopoulos, Catal. Today 180 (2012) 68–80.
[42] L. Barelli, G. Bidini, F. Gallorini, S. Servili, Energy 33 (2008) 554–570.
[43] D.P. Harrison, Ind. Eng. Chem. Res. 47 (2008) 6486–6501.
[44] B. Balasubramanian, A. Lopez Ortiz, S. Kaytakoglu, D.P. Harrison, Chem. Eng. Sci. 54 (1999) 3543–3552.
[45] D.M. Ruthven, Principles of Adsorption and Adsorption Processes, Wiley, 2016, pp. 1984.
[46] R.F.P.M. Moreira, J.L. Soares, G.L. Casarin, A.E. Rodrigues, Sep. Sci. Technol. 41 (2006) 341–357.
[47] B. Ficicilar, T. Dogu, Catal. Today 115 (2006) 274–278.
[48] J. Boon, P.D. Cobden, H.A.J. van Dijk, M. van Sint Annaland, Chem. Eng. Sci. 122 (2015) 219–231.
[49] D. Jansen, E. van Selow, P. Cobden, G. Manzolini, E. Macchi, M. Gazzani, R. Blom, P.P. Henriksen, R. Beavis, A. Wright, Energy Procedia 37 (2013) 2265–2273.
[50] E.R. van Selow, P.D. Cobden, P.A. Verbraeken, J.R. Hufton, R.W. van den Brink, Ind. Eng. Chem. Res. 48 (2009) 4184–4193.
[51] J. Boon, P.D. Cobden, H.A.J. van Dijk, C. Hoogland, E.R. van Selow, M. van Sint Annaland, Chem. Eng. J. 248 (2014) 406–414.
[52] P. Mierczynski, W. Maniukiewicz, T. Maniecki, Cent. Eur. J. Chem. 11 (2013) 912–919.
[53] F. Huber, H. Meland, M. Rønning, H. Venvik, A. Holmen, Top. Catal. 45 (2007) 101–104.
[54] T.P. Maniecki, P. Mierczyński, W.K. Jóźwiak, Kinet. Catal. 51 (2010) 843–848.
[55] Y. Zhang, C. Chen, X. Lin, D. Li, X. Chen, Y. Zhan, Q. Zheng, Int. J. Hydrogen Energy 39 (2014) 3746–3754.
[56] A. Budiman, M. Ridwan, S.M. Kim, J.-W. Choi, C.W. Yoon, J.-M. Ha, D.J. Suh, Y.-W. Suh, Appl. Catal. A 462–463 (2013) 220–226.
[57] M.A. Soria, S. Tosti, A. Mendes, L.M. Madeira, Fuel 159 (2015) 854–863.
[58] F. Meshkani, M. Rezaei, J. Ind. Eng. Chem. 30 (2015) 353–358.
[59] K. Sagata, Y. Kaneda, H. Yamaura, S. Kobayashi, H. Yahiro, Int. J. Hydrogen Energy 39 (2014) 20639–20645.
[60] A. Jha, D.-W. Jeong, W.-J. Jang, Y.-L. Lee, H.-S. Roh, Int. J. Hydrogen Energy 40 (2015) 9209–9216.
[61] J. Kugai, E.B. Fox, C. Song, Appl. Catal. A 497 (2015) 31–41.
[62] D. Li, Y. Cai, Y. Ding, R. Li, M. Lu, L. Jiang, Int. J. Hydrogen Energy 40 (2015) 10016–10025.
[63] D.-W. Jeong, W.-J. Jang, J.-O. Shim, W.-B. Han, H.-S. Roh, U.H. Jung, W.L. Yoon, Renew. Energy 65 (2014) 102–107.
[64] R.J. Madon, D. Braden, S. Kandoi, P. Nagel, M. Mavrikakis, J.A. Dumesic, J. Catal. 281 (2011) 1–11.
[65] L. Li, L. Song, C. Chen, Y. Zhang, Y. Zhan, X. Lin, Q. Zheng, H. Wang, H. Ma, L. Ding, W. Zhu, Int. J. Hydrogen Energy 39 (2014) 19570–19582.
[66] O. Arbeláez, T.R. Reina, S. Ivanova, F. Bustamante, A.L. Villa, M.A. Centeno, J.A. Odriozola, Appl. Catal. A 497 (2015) 1–9.
[67] P.V.D.S. Gunawardana, H.C. Lee, D.H. Kim, Int. J. Hydrogen Energy 34 (2009) 1336–1341.
[68] F. Meshkani, M. Rezaei, Renew. Energy 74 (2015) 588–598.
[69] K. Sagata, N. Imazu, H. Yahiro, Catal. Today 201 (2013) 145–150.
[70] X. Lin, R. Li, Y. Zhang, Y. Zhan, C. Chen, Q. Zheng, J. Ma, Inter. J. Hydrogen Energy 40 (2015) 1735–1741.
[71] C. Chen, C. Ruan, Y. Zhan, X. Lin, Q. Zheng, K. Wei, Int. J. Hydrogen Energy 39 (2014) 317–324.
[72] J.A.C. Silva, A.F. Cunha, K. Schumann, A.E. Rodrigues, Microporous Mesoporous Mater. 187 (2014) 100–107.
[73] A.F. Cunha, Y.J. Wu, J.C. Santos, A.E. Rodrigues, Ind. Eng. Chem. Res. 51 (2012) 13132–13143.
[74] weblink https://www.ecn.nl/docs/library/report/2013/l13032.pdf.
[75] weblink http://www.jmprotech.com/images-uploaded/files/JM%20Hydrogen%20Brochure.pdf.
[76] M.V. Twigg, M.S. Spencer, Top. Catal. 22 (2003) 191–203.
[77] N.K. Das, A.K. Dalai, R. Ranganathan, Can. J. Chem. Eng. 85 (2007) 92–100.
[78] J.-H. Lin, V.V. Guliants, ChemCatChem 3 (2011) 1426–1430.
[79] D.-W. Jeong, W.-J. Jang, H.-S. Na, J.-O. Shim, A. Jha, H.-S. Roh, J. Ind. Eng. Chem. 27 (2015) 35–39.
[80] P. Mierczynski, T. Maniecki, W. Maniukiewicz, W. Jozwiak, React. Kinet. Mech. Catal. 104 (2011) 139–148.